Quantum control of a nanoparticle optically levitated in cryogenic free-space

Lukas Novotny (lnovotny@ethz.ch)
ETH Zurich https://orcid.org/0000-0002-9970-8345
Felix Tebbenjohanns
ETH Zurich
Maria Luisa Mattana
ETH Zurich
Massimiliano Rossi
ETH https://orcid.org/0000-0001-8992-3378
Martin Frimmer
ETH Zurich

Physical Sciences - Article

Keywords: Mechanical Motion Decoherence, Micromechanical Oscillator, Measurement-based Feedback, Matter-wave Experiments, Macroscopic Scales

Posted Date: March 10th, 2021

DOI: https://doi.org/10.21203/rs.3.rs-298193/v1

Version of Record: A version of this preprint was published at Nature on July 14th, 2021. See the published version at https://doi.org/10.1038/s41586-021-03617-w.

Quantum control of a nanoparticle optically levitated in cryogenic free space

Felix Tebbenjohanns,* Maria Luisa Mattana,* Massimiliano Rossi,* Martin Frimmer, and Lukas Novotny
Photonics Laboratory, ETH Zürich, CH-8093 Zürich, Switzerland
(Dated: March 4, 2021)

Tests of quantum mechanics on a macroscopic scale require extreme control over mechanical motion and its decoherence [1–4]. Quantum control of mechanical motion has been achieved by engineering the radiation-pressure coupling between a micromechanical oscillator and the electromagnetic field in a resonator [5–8]. Furthermore, measurement-based feedback control relying on cavity-enhanced detection schemes has been used to cool micromechanical oscillators to their quantum ground states [9]. In contrast to mechanically tethered systems, optically levitated nanoparticles are particularly promising candidates for matter-wave experiments with massive objects [10, 11], since their trapping potential is fully controllable. In this work, we optically levitate a femto-gram dielectric particle in cryogenic free space, which suppresses thermal effects sufficiently to make the measurement backaction the dominant decoherence mechanism. With an efficient quantum measurement, we exert quantum control over the dynamics of the particle. We cool its center-of-mass motion by measurement-based feedback to an average occupancy of 0.65 motional quanta, corresponding to a state purity of 43%. The absence of an optical resonator and its bandwidth limitations holds promise to transfer the full quantum control available for electromagnetic fields to a mechanical system. Together with the fact that the optical trapping potential is highly controllable, our experimental platform offers a route to investigating quantum mechanics at macroscopic scales [12, 13].

Introduction. Mechanical oscillators with small dissipation have become indispensable tools for sensing and signal transduction [14–18]. In optomechanics, such oscillators are coupled to a light field to read out and control the mechanical motion at the fundamental limits set by quantum theory [8]. A landmark feat in this context has been cavity-cooling of micromechanical oscillators to their quantum ground state of motion using dynamical backaction [5, 6].

The remarkable success of cavity optomechanics as a technology platform attracted the attention of a scientific community seeking to test the limitations of quantum theory at macroscopic scales [13, 19–22]. A particularly exciting idea is to delocalize the wave function of a massive object over a distance larger than its physical size [12]. This regime is outside the scope of mechanically clamped oscillators and requires systems with largely tunable potentials, such as dielectric particles levitated in an optical trap [10, 11]. The optical intensity distribution in a laser focus forms a controllable conservative potential for the particle's center-of-mass motion [23]. A prerequisite for investigating macroscopic quantum effects is to prepare the particle in a quantum mechanically pure state, such as its motional ground state. Subsequently, the trapping potential can be switched off [24], allowing for coherent evolution of the particle in the absence of decoherence generated by photon recoil heating [25, 26]. Furthermore, other sources of decoherence, such as collisions with gas molecules and recoil from blackbody photons, must be excluded [27, 28]. A cryogenic environment can provide both the required extreme high vacuum and the sufficiently low thermal population of the electromagnetic continuum.

Cavity-control of the center-of-mass motion of a levitated particle has made tremendous progress in recent years [29–31], and ground-state cooling by dynamical back-action has recently been reported [32]. An alternative approach to purify the particle's motional state relies on measurement-based feedback [23, 33–37]. To operate this technique in the quantum regime requires performing a measurement whose quantum backaction represents the dominant disturbance of the system [25, 26]. In addition, the result of this measurement needs to be recorded with sufficient efficiency, to compensate the measurement backaction by the feedback system [9, 38, 39]. Borrowing techniques developed for tethered optomechanical systems [9, 39–41], levitated particles have been feedback-cooled to single-digit phonon occupation numbers [42], where first signatures of their motional ground state have been observed [43]. These studies suggest that ground-state cooling of mechanical motion without enhancing light-matter interaction with an optical resonator is possible with sufficiently high detection efficiency. Such a cavity-free optomechanical system would be unrestricted by the limitations regarding bandwidth, stability, and mode-matching associated with an optical resonator.

In this work, we optically levitate a nanoparticle in a cryogenic environment and feedback-cool its motion to the quantum ground state. Our feedback control relies on a cavity-free optical measurement of the particle position that approaches the minimum of the Heisenberg relation to within a factor of two.

Experimental system. In Fig. 1a we show our experimental system. We generate a single-beam dipole trap by strongly focusing a laser ($P_t \sim 1.2$ W, wavelength $\lambda = 1550$ nm, linearly polarized along the x axis) with

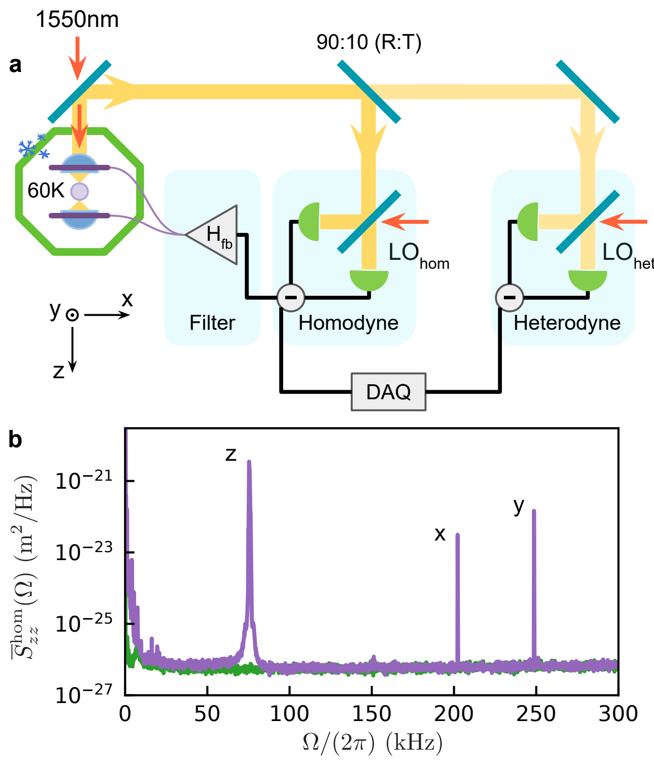

Figure 1. **Experimental setup.** **(a)** An electrically charged silica nanoparticle is optically levitated in a cryogenic environment. The light scattered back by the particle is split between the heterodyne and the homodyne receivers. The homodyne signal is filtered, and fed back as an electric force to the particle to cool its center-of-mass motion along the optical axis. **(b)** Power spectral density of the parametrically pre-cooled center-of-mass oscillation modes (purple) along the z, x, and y axis (at 77 kHz, 202 kHz, and 249 kHz, respectively). In green we plot the LO noise floor.

an aspheric trapping lens (numerical aperture 0.75). A dipolar dielectric scatterer in the focal region experiences a three-dimensional confining potential, which is harmonic for small displacements from the focal center. In our experiments, we trap a single, electrically charged spherical silica nanoparticle (diameter 100 nm, mass $m \sim 1$ fg). The resonance frequency of the particle's center-of-mass motion along the optical axis z is $\Omega_z/(2\pi) = 77.6$ kHz (see Fig. 1b). The resonance frequencies in the focal plane are $\Omega_{\rm x}/(2\pi) = 202$ kHz along and $\Omega_{\rm y}/(2\pi) = 249$ kHz perpendicular to the axis of polarization.

To suppress heating due to collisions with gas molecules, we operate our optical trap inside a 4 K cryostat. On the holder of the trapping lens, we measure a temperature of 60 K, which results from heating due to residual optical absorption (see Supplementary). The cryogenic environment reduces the thermal energy of the gas molecules, and simultaneously lowers the gas pressure by cryogenic pumping. An ionization gauge located in the outer chamber (at 295 K) of the cryostat reads a pressure of 3×10^{-9} mbar, which we treat as an upper bound for the pressure at the location of the particle. To stabilize the particle inside the trap and to avoid nonlinearities of the trapping potential, we pre-cool the particle's motion in the three dimensions using parametric feedback [34]. In the following, we focus our attention on the motion along the optical z axis.

The detection of the particle's motion relies on the fact that its position is predominantly encoded in the phase of the light scattered back into the trapping lens [44]. This backscattered field is directed by an optical circulator to the detection setup, where 90% (10%) of the signal is sent to a homodyne (heterodyne) receiver. These receivers convert the phase of the optical field into an electrical signal. We use the homodyne measurement for feedback-control, and the heterodyne signal for an independent out-of-loop measurement of the particle's motion.

Feedback cooling to the ground state. Our experimental platform is a cavity-free optomechanical system, performing a continuous measurement of the displacement of the particle [8, 10]. According to quantum theory, this measurement inevitably entails a backaction. For the levitated particle, this quantum backaction is associated with the radiation pressure shot noise arising from the quantization of the light field's linear momentum [26]. Importantly, with a sufficiently efficient detection system in place (see Supplementary), it is possible to apply a feedback force to the particle that fully balances the effect of the backaction [9, 38, 40].

We deploy a feedback method termed *cold damping* [38, 45]. In this scheme, a viscous feedback force is derived from the measurement signal, increasing the dissipation while adding a minimum amount of fluctuations. Our feedback circuit is a digital filter that electronically processes the homodyne signal in real-time. The filter mainly comprises a delay line to shift the phase of the frequencies near Ω_z by $\pi/2$ (see Supplementary). This procedure exploits the particle's harmonic motion to estimate the velocity from the measured displacement. The filtered signal is applied as a voltage to a pair of electrodes located near the nanoparticle, actuating the feedback via the Coulomb force.

We now turn to the analysis of the particle's motional energy under feedback. Our first method to extract the phonon population of the particle relies on Raman sideband thermometry [43, 46, 47]. To this end, we analyze the signal recorded on the heterodyne receiver (see Supplementary), which provides an out-of-loop measurement of the motion of the particle [37]. The power spectral density (PSD) [48] of both the red-shifted Stokes sideband $\bar{S}_{rr}(\Omega)$ and of the blue-shifted anti-Stokes sideband $\bar{S}_{bb}(\Omega)$ (Fig. 2a) show a Lorentzian lineshape on top of a white noise floor. Importantly, the total noise power in the two sidebands is visibly different. From this sideband

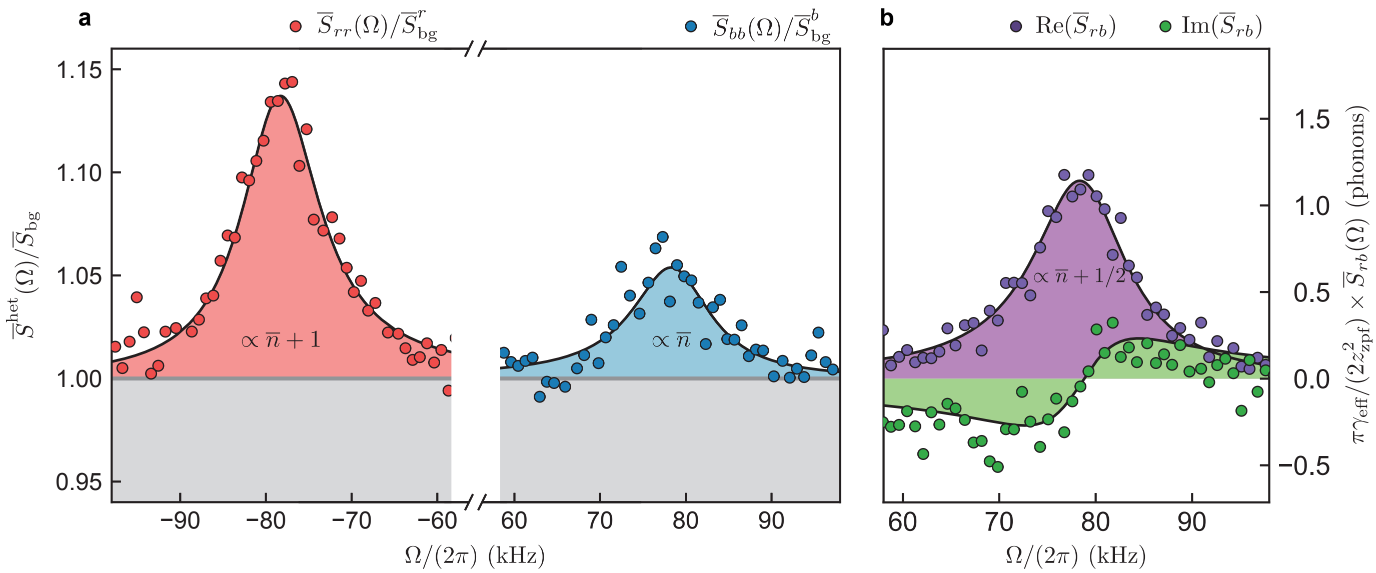

Figure 2. **Quantum ground state verification via out-of-loop measurements.** **(a)** Stokes (red circles) and anti-Stokes (blue circles) sidebands measured by the out-of-loop heterodyne detector, at the largest electronic feedback gain. The black lines are fits to Eqs. (1), from which we extract the sideband powers. From their ratio, we extract a final occupation of $\bar{n} = 0.66 \pm 0.08$. **(b)** Real (purple circles) and imaginary (green circles) parts of the cross-power spectral density between the Stokes and anti-Stokes sideband, together with theoretical fits (black lines). We calibrate the vertical axis using the imaginary part, and we extract a final occupation of $\bar{n} = 0.64 \pm 0.09$ from the real part.

asymmetry, we can extract the phonon population by fitting our data to the expressions

$$\bar{S}_{rr}(\Omega) = \bar{S}^{r}_{\rm bg} + R|\chi_{\rm eff}(\Omega)|^2(\bar{n}+1), \qquad (1a)$$

$$\bar{S}_{bb}(\Omega) = \bar{S}^{b}_{\rm bg} + R|\chi_{\rm eff}(\Omega)|^2\bar{n}, \qquad (1b)$$

with $\bar{S}^{r,b}_{\rm bg}$ the spectral background floor, $R = m\gamma_{\rm eff}\hbar\Omega_{\rm z}/\pi$ a scaling factor, $\chi_{\rm eff}(\Omega) = m^{-1}/(\Omega^2_{\rm z} - \Omega^2 - \mathrm{i}\gamma_{\rm eff}\Omega)$ the effective mechanical susceptibility modified by the feedback, $\gamma_{\rm eff}$ the effective linewidth including the broadening due to feedback, and $\bar{n}$ the average phonon occupation of the mechanical state.

From the fit of our data (solid lines in Fig. 2a), we extract a linewidth of $\gamma_{\rm eff}/(2\pi) = 11.1$ kHz together with a residual occupation of $\bar{n} = 0.66 \pm 0.08$, corresponding to a ground-state occupancy of $1/(\bar{n}+1) = 60\%$. The error is obtained by propagating the standard deviation (s.d.) of the fitted areas. We note that the method of Raman thermometry does not rely on any calibration of the system. Instead, it is the zero-point energy of the oscillator which serves as the absolute scale all energies are measured against.

As a second method to infer the residual phonon population of the particle under feedback, we analyze the cross-correlations between the two measured sidebands [49, 50]. In Fig. 2b, we show the real part of the measured cross correlation $\mathrm{Re}(S_{\rm rb})$ (purple) and its imaginary part $\mathrm{Im}(S_{\rm rb})$ (green). We fit the data to a theoretical model given by (see Supplementary)

$$\bar{S}_{rb}(\Omega) = R|\chi_{\rm eff}(\Omega)|^2 \left(\bar{n} + \frac{1}{2} + \frac{\mathrm{i}}{2}\frac{\Omega^2 - \Omega^2_{\rm z}}{\gamma_{\rm eff}\Omega_{\rm z}}\right). \qquad (2)$$

Importantly, the imaginary part of the cross-correlation is independent of the phonon population $\bar{n}$. It arises purely from the zero-point fluctuations and can thus serve to calibrate the real part, from which we extract a phonon occupation of $\bar{n} = 0.64 \pm 0.09$. The error is obtained from the propagation of the uncertainties (s.d.) in the fitted parameters. This result is well in agreement with the value extracted from the sideband asymmetry.

Quantum measurement. Efficient quantum measurement is a prerequisite for stabilizing the levitated nanoparticle in its quantum ground state via feedback. In the following, we perform a detailed analysis of our measurement system. To this end, we analyze the measurement record of our in-loop homodyne receiver and derive the measurement efficiency $\eta_{\rm meas}$, that is, the amount of information gathered per disturbance incurred [51]. In Fig. 3a we show, in dark red, the homodyne spectrum acquired at the lowest feedback gain labelled by the set gain $g_{\rm el} = 0$ dB ($\gamma_{\rm eff} = 2\pi \times 21.9$ Hz). At such low gain, the measured fluctuations on resonance largely exceed the imprecision noise and the feedback solely leads to a broadening of the mechanical susceptibility. In this regime, the imprecision noise fed back as a force does not play any role, and can be safely ignored. Upon calibration via an out-of-loop energy measurement at a moderate gain (at $g_{\rm el} = 25$ dB), we fit

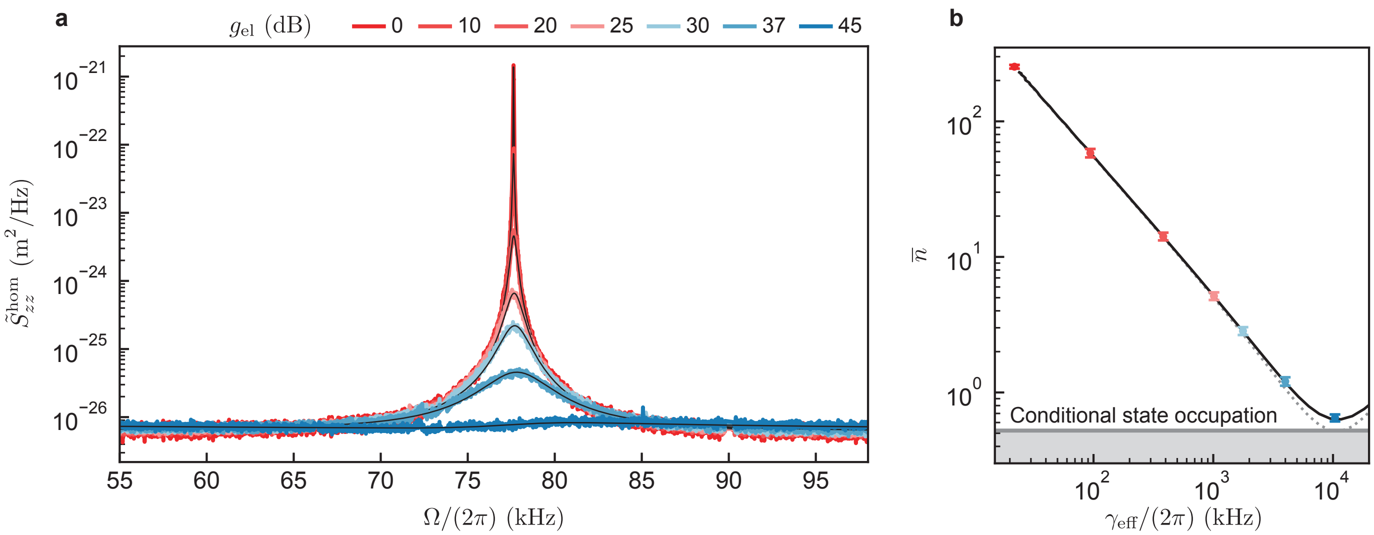

Figure 3. **In-loop analysis of the feedback system. (a)** Single-sided displacement spectra measured by the in-loop homodyne detector, at different electronic gains g_{el}. We exclude three narrow spectral features from the analysis (see Supplementary). The black lines are fits to a theoretical model (see Supplementary). **(b)** Mechanical occupations extracted from integrating the computed position and momentum spectra, which are based on parameters estimated from the in-loop spectra. The solid black (dotted grey) line is a theoretical model assuming an ideal delay filter (cold damping). The horizontal grey line corresponds to the occupation of the conditional state, stemming from the performed measurements. The error bars reflect the standard deviation (s.d.) in the fitted parameters, as well as the statistical error on the calibration method.

the observed spectrum to (see Supplementary)

$$\bar{S}_{zz}^{\mathrm{hom}}(\Omega) = \bar{S}_{\mathrm{imp}} + |\chi_{\mathrm{eff}}(\Omega)|^2 \bar{S}_{FF}^{\mathrm{tot}}, \qquad (3)$$

where $\bar{S}_{FF}^{\mathrm{tot}} = \hbar^2\Gamma_{\mathrm{tot}}/(2\pi z_{\mathrm{zpf}}^2)$ is the total force noise PSD, $\bar{S}_{\mathrm{imp}} = z_{\mathrm{zpf}}^2/(8\pi\Gamma_{\mathrm{meas}})$ is the imprecision noise PSD, and $z_{\mathrm{zpf}}^2 = \hbar/(2m\Omega_{\mathrm{z}})$ denotes the zero-point fluctuations of the oscillator. We note that these two spectral densities can be equivalently written in terms of a measurement rate $\Gamma_{\mathrm{meas}} = \eta_d\Gamma_{\mathrm{qba}}$ (with Γ_{qba} the decoherence rate due to the quantum backaction, and η_d the overall detection efficiency), and a total decoherence rate $\Gamma_{\mathrm{tot}} = \Gamma_{\mathrm{qba}} + \Gamma_{\mathrm{exc}} = \gamma_{\mathrm{eff}}(\bar{n}+1/2)$ (with Γ_{exc} the decoherence rate in excess of quantum backaction). From the fit, we extract a measurement rate of $\Gamma_{\mathrm{meas}}/(2\pi) = (1.33 \pm 0.04)$ kHz and a total decoherence rate of $\Gamma_{\mathrm{tot}}/(2\pi) = (5.5 \pm 0.3)$ kHz. The measurement rate approaches the total decoherence rate, giving a measurement efficiency of $\eta_{\mathrm{meas}} = \Gamma_{\mathrm{meas}}/\Gamma_{\mathrm{tot}} = 0.24 \pm 0.02$, which is bounded by $\eta_{\mathrm{meas}} \leq 1$ according to the Heisenberg measurement-disturbance relation [46, 51, 52].

Next, we characterize the role of the feedback gain in our system. To this end, we record homodyne spectra at increasing gain settings, as shown in Fig. 3a. For small gain values, the feedback only increases the mechanical linewidth. For high gain values however, the spectra flatten and even dip below the imprecision noise, an effect known as *noise squashing* [40]. In this case, the feedback-induced correlations become dominant and increase the displacement fluctuations, rather than reducing them. We fit each spectrum to a full in-loop model, where we independently characterize the transfer function of the electronic loop (see Supplementary). Then, we use the results of the fits to compute the effective linewidths and the phonon occupations, shown in Fig. 3b. At the highest gain, we estimate an occupation of $\bar{n} = (0.65 \pm 0.04)$, consistent with both other methods described above. Based on the estimated measurement and total decoherence rates, we calculate a theoretical model for the occupations under a pure delay filter (black line in Fig. 3b). For comparison, we show the theoretical results achievable under ideal cold damping [38] in the limit of $\gamma_{\mathrm{eff}} \ll \Omega_{\mathrm{z}}$ (dotted grey line). In this case, an induced linewidth of γ_{eff} corresponds to an occupation $\bar{n} = \Gamma_{\mathrm{tot}}/\gamma_{\mathrm{eff}} + \gamma_{\mathrm{eff}}/(16\Gamma_{\mathrm{meas}}) - 1/2$ [37], dependent only on the measurement and decoherence rates.

Discussion and outlook. In summary, we have achieved quantum control over the motion of a levitated nanosphere. This control relies on the high reported measurement efficiency of 24%, comparable to what has been achieved with tethered micromechanical resonators [9], atomic systems [53], and superconducting circuits [54]. As an example of measurement-based quantum control, we have experimentally stabilized the nanoparticle's motion in its quantum ground state via active feedback. The prepared quantum state has a residual occupation of $\bar{n} = 0.65$ phonons, corresponding to a purity of $1/(1+2\bar{n}) = 43\%$. Under optimal control, achievable by optimization of the feedback circuit, we expect to reach the same occupation as the conditional state [51, 55], that is, $\bar{n}_{\mathrm{cond}} \approx (1/\sqrt{\eta_{\mathrm{meas}}} -$

$1)/2 = 0.5$ (see Fig. 3b). Our experiment approaches this limit to within 30%. Notably, this is the first time that quantum control of mechanical degrees of freedom has been achieved without the use of an optical resonator. Our cavity-free platform allows overcoming the bistability in continuously operated optomechanical cavities, which limits the fastest achievable control time, $1/\Gamma_{\rm qba}$, to roughly the mechanical oscillation period $2\pi/\Omega_z$ [8]. The control time $1/\Gamma_{\rm qba}$ is inversely proportional to the particle's volume. When the excess decoherence is negligible, we expect to achieve $1/\Gamma_{\rm qba} \approx 1/\Gamma_{\rm tot} = 1\,\mu$s for a 300-nm-diameter nanosphere, well below the measured period of $2\pi/\Omega_z = 13\,\mu$s. This opens the door for fast continuous and pulsed displacement measurement [56, 57].

Importantly, we conduct levitated-optomechanics experiments in a cryogenic environment for the first time. This represents a milestone towards the generation of genuine macroscopic quantum states of a nanosphere, which would require extremely low levels of decoherence [12]. On the one hand, cryogenic pumping can achieve extreme-high-vacuum in excess of 10^{-17} mbar [58], suppressing decoherence due to gas collisions. On the other hand, silica nanospheres quickly thermalize at the temperature of the surrounding cryogenic environment once the laser is switched off. This drastically reduces the decoherence due to emission of blackbody photons. For a trapping field intensity of 300 mW/μm^2, the bulk heating rate due to optical absorption is estimated to be approximately 2 K/ms [59]. By switching on the optical field only for the needed duration of $1/\Gamma_{\rm meas} \approx 100\ \mu$s to stabilize the ground state [60], we can maintain the internal temperature of the nanosphere in equilibrium with the surrounding cryogenic environment. At the measured temperature of 60 K and at a pressure of 10^{-12} mbar, well within the reach of state-of-the-art cryostats [61], we estimate a coherent evolution time of around 50 ms [28]. This would be sufficient to coherently expand the quantum wave function up to a size comparable with the nanosphere itself, opening the doors for exploring macroscopic quantum effects [62].

Acknowledgments This research was supported by the NCCR-QSIT program (Grant No. 51NF40-160591), and SNF (Grant No. 200021L-16931 and Grant No. 206021-189605). We are grateful to F. van der Laan for his contributions to the particle characterization procedure. We thank O. Wipfli and C. Fischer for their suggestions in designing the cryogenic vacuum chamber, J. Piotrowski and D. Windey for their advise with the trap assembly, and Y. Li for her work on the control software. We thank our colleagues P. Back, E. Bonvin, J. Gao, A. Militaru, R. Reimann, J. Vijayan, and J. Zielinska for input and discussions.

---

* These authors contributed equally to this work.

[1] W. H. Zurek, "Decoherence and the transition from quantum to classical — revisited," in *Quantum Decoherence: Poincaré Seminar 2005*, edited by B. Duplantier, J.-M. Raimond, and V. Rivasseau (Birkhäuser Basel, Basel, 2007) pp. 1–31.
[2] Y. Chen, Journal of Physics B: Atomic, Molecular and Optical Physics **46**, 104001 (2013).
[3] M. Arndt, O. Nairz, J. Vos-Andreae, C. Keller, G. V. D. Zouw, and A. Zeilinger, Nature **401**, 680–682 (1999).
[4] K. Hornberger, S. Gerlich, P. Haslinger, S. Nimmrichter, and M. Arndt, Rev. Mod. Phys. **84**, 157 (2012).
[5] J. D. Teufel, T. Donner, D. Li, J. W. Harlow, M. S. Allman, K. Cicak, A. J. Sirois, J. D. Whittaker, K. W. Lehnert, and R. W. Simmonds, Nature **475**, 359 (2011).
[6] J. Chan, T. P. M. Alegre, A. H. Safavi-Naeini, J. T. Hill, A. Krause, S. Gröblacher, M. Aspelmeyer, and O. Painter, Nature **478**, 89–92 (2011).
[7] L. Qiu, I. Shomroni, P. Seidler, and T. J. Kippenberg, Phys. Rev. Lett. **124**, 173601 (2020).
[8] M. Aspelmeyer, T. J. Kippenberg, and F. Marquardt, Rev. Mod. Phys. **86**, 1391 (2014).
[9] M. Rossi, D. Mason, J. Chen, Y. Tsaturyan, and A. Schliesser, Nature **563**, 53–58 (2018).
[10] D. E. Chang, C. A. Regal, S. B. Papp, D. J. Wilson, J. Ye, O. Painter, H. J. Kimble, and P. Zoller, Proc. Natl. Acad. Sci. USA **107**, 1005 (2010).
[11] O. Romero-Isart, M. L. Juan, R. Quidant, and J. I. Cirac, New Journal of Physics **12**, 033015 (2010).
[12] O. Romero-Isart, A. C. Pflanzer, F. Blaser, R. Kaltenbaek, N. Kiesel, M. Aspelmeyer, and J. I. Cirac, Phys. Rev. Lett. **107**, 020405 (2011).
[13] A. J. Leggett, Journal of Physics: Condensed Matter **14**, R415 (2002).
[14] V. B. Braginskii and A. B. Manukin, *Measurement of weak forces in physics experiments / V. B. Braginsky and A. B. Manukin ; edited by David H. Douglass* (University of Chicago Press Chicago, 1977).
[15] E. Verhagen, S. Deléglise, S. Weis, A. Schliesser, and T. J. Kippenberg, Nature **482**, 63–67 (2012).
[16] R. W. Andrews, R. W. Peterson, T. P. Purdy, K. Cicak, R. W. Simmonds, C. A. Regal, and K. W. Lehnert, Nature Physics **10**, 321 (2014).
[17] T. Bagci, A. Simonsen, S. Schmid, L. G. Villanueva, E. Zeuthen, J. Appel, J. M. Taylor, A. Sørensen, K. Usami, A. Schliesser, and E. S. Polzik, Nature **507**, 81 (2014).
[18] M. Mirhosseini, A. Sipahigil, M. Kalaee, and O. Painter, Nature **588**, 599 (2020).
[19] J. I. Cirac, M. Lewenstein, K. Mølmer, and P. Zoller, Phys. Rev. A **57**, 1208 (1998).
[20] S. Bose, K. Jacobs, and P. L. Knight, Phys. Rev. A **59**, 3204 (1999).
[21] A. J. Leggett and A. Garg, Phys. Rev. Lett. **54**, 857 (1985).
[22] W. Marshall, C. Simon, R. Penrose, and D. Bouwmeester, Phys. Rev. Lett. **91**, 130401 (2003).
[23] A. Ashkin and J. M. Dziedzic, Appl. Phys. Lett. **30**, 202 (1977).
[24] E. Hebestreit, M. Frimmer, R. Reimann, C. Dellago, F. Ricci, and L. Novotny, Rev. Sci. Instr. **89**, 033111 (2018).
[25] T. P. Purdy, R. W. Peterson, and C. A. Regal, Science **339**, 801 (2013).
[26] V. Jain, J. Gieseler, C. Moritz, C. Dellago, R. Quidant, and L. Novotny, Phys. Rev. Lett. **116**, 243601 (2016).

[27] R. Kaltenbaek, G. Hechenblaikner, N. Kiesel, O. Romero-Isart, K. C. Schwab, U. Johann, and M. Aspelmeyer, Experimental Astronomy **34**, 123 (2012).

[28] O. Romero-Isart, Phys. Rev. A **84**, 052121 (2011).

[29] N. Kiesel, F. Blaser, U. Delić, D. Grass, R. Kaltenbaek, and M. Aspelmeyer, Proc. Natl. Acad. Sci. USA **110**, 14180 (2013).

[30] D. Windey, C. Gonzalez-Ballestero, P. Maurer, L. Novotny, O. Romero-Isart, and R. Reimann, Phys. Rev. Lett. **122**, 123601 (2019).

[31] U. Delić, M. Reisenbauer, D. Grass, N. Kiesel, V. Vuletić, and M. Aspelmeyer, Phys. Rev. Lett. **122**, 123602 (2019).

[32] U. Delić, M. Reisenbauer, K. Dare, D. Grass, V. Vuletić, N. Kiesel, and M. Aspelmeyer, Science **367**, 892 (2020).

[33] T. Li, S. Kheifets, and M. G. Raizen, Nat. Phys. **7**, 527 (2011).

[34] J. Gieseler, B. Deutsch, R. Quidant, and L. Novotny, Phys. Rev. Lett. **109**, 103603 (2012).

[35] M. Iwasaki, T. Yotsuya, T. Naruki, Y. Matsuda, M. Yoneda, and K. Aikawa, Phys. Rev. A **99**, 051401 (2019).

[36] G. P. Conangla, F. Ricci, M. T. Cuairan, A. W. Schell, N. Meyer, and R. Quidant, Phys. Rev. Lett. **122**, 223602 (2019).

[37] F. Tebbenjohanns, M. Frimmer, A. Militaru, V. Jain, and L. Novotny, Phys. Rev. Lett. **122**, 223601 (2019).

[38] S. Mancini, D. Vitali, and P. Tombesi, Phys. Rev. Lett. **80**, 688 (1998).

[39] D. Wilson, V. Sudhir, N. Piro, R. Schilling, A. Ghadimi, and T. J. Kippenberg, Nature **524**, 325 (2015).

[40] P. F. Cohadon, A. Heidmann, and M. Pinard, Phys. Rev. Lett. **83**, 3174 (1999).

[41] M. Poggio, C. L. Degen, H. J. Mamin, and D. Rugar, Phys. Rev. Lett. **99**, 017201 (2007).

[42] M. Kamba, H. Kiuchi, T. Yotsuya, and K. Aikawa, (2020), arXiv:2011.12507.

[43] F. Tebbenjohanns, M. Frimmer, V. Jain, D. Windey, and L. Novotny, Phys. Rev. Lett. **124**, 013603 (2020).

[44] F. Tebbenjohanns, M. Frimmer, and L. Novotny, Phys. Rev. A **100**, 043821 (2019).

[45] C. Genes, D. Vitali, P. Tombesi, S. Gigan, and M. Aspelmeyer, Phys. Rev. A **77**, 033804 (2008).

[46] A. A. Clerk, M. H. Devoret, S. M. Girvin, F. Marquardt, and R. J. Schoelkopf, Rev. Mod. Phys. **82**, 1155 (2010).

[47] A. H. Safavi-Naeini, J. Chan, J. T. Hill, T. P. M. Alegre, A. Krause, and O. Painter, Phys. Rev. Lett. **108**, 033602 (2012).

[48] We define our two-sided, symmetrized PSDs $\bar{S}_{zz}(\Omega)$ and our single-sided PSDs $\tilde{S}_{zz}(f) = 4\pi\bar{S}_{zz}(2\pi f)$ according to $\langle z^2\rangle = \int_{-\infty}^{\infty} \mathrm{d}\Omega\, \bar{S}_{zz}(\Omega) = \int_0^{\infty} \mathrm{d}f\, \tilde{S}_{zz}(f)$.

[49] T. P. Purdy, K. E. Grutter, K. Srinivasan, and J. M. Taylor, Science **356**, 1265 (2017).

[50] A. B. Shkarin, A. D. Kashkanova, C. D. Brown, S. Garcia, K. Ott, J. Reichel, and J. G. E. Harris, Phys. Rev. Lett. **122**, 153601 (2019).

[51] H. M. Wiseman and G. J. Milburn, *Quantum Measurement and Control* (Cambridge University Press, 2010).

[52] V. B. Braginsky and F. Y. Khalili, *Quantum Measurement* (Cambridge University Press, Cambridge, 1992).

[53] C. Sayrin, I. Dotsenko, X. Zhou, B. Peaudecerf, T. Rybarczyk, S. Gleyzes, P. Rouchon, M. Mirrahimi, H. Amini, M. Brune, and et al., Nature **477**, 73–77 (2011).

[54] R. Vijay, C. Macklin, D. H. Slichter, S. J. Weber, K. W. Murch, R. Naik, A. N. Korotkov, and I. Siddiqi, Nature **490**, 77–80 (2012).

[55] A. C. Doherty and K. Jacobs, Phys. Rev. A **60**, 2700 (1999).

[56] C. Meng, G. A. Brawley, J. S. Bennett, M. R. Vanner, and W. P. Bowen, Phys. Rev. Lett. **125**, 043604 (2020).

[57] M. R. Vanner, I. Pikovski, G. D. Cole, M. S. Kim, Č. Brukner, K. Hammerer, G. J. Milburn, and M. Aspelmeyer, Proc. Natl. Acad. Sci. USA **108**, 16182 (2011).

[58] G. Gabrielse, X. Fei, L. A. Orozco, R. L. Tjoelker, J. Haas, H. Kalinowsky, T. A. Trainor, and W. Kells, Phys. Rev. Lett. **65**, 1317 (1990).

[59] J. Bateman, S. Nimmrichter, K. Hornberger, and H. Ulbricht, Nat. Commun. **5**, 4788 (2014).

[60] A. C. Doherty, S. M. Tan, A. S. Parkins, and D. F. Walls, Phys. Rev. A **60**, 2380 (1999).

[61] P. Micke, J. Stark, S. A. King, T. Leopold, T. Pfeifer, L. Schmöger, M. Schwarz, L. J. Spieß, P. O. Schmidt, J. R. C. López-Urrutia, and et al., Rev. Sci. Instr. **90**, 065104 (2019).

[62] R. Kaltenbaek, M. Aspelmeyer, P. F. Barker, A. Bassi, J. Bateman, K. Bongs, S. Bose, C. Braxmaier, Č. Brukner, B. Christophe, M. Chwalla, P.-F. Cohadon, A. M. Cruise, C. Curceanu, K. Dholakia, L. Diósi, K. Döringshoff, W. Ertmer, J. Gieseler, N. Gürlebeck, G. Hechenblaikner, A. Heidmann, S. Herrmann, S. Hossenfelder, U. Johann, N. Kiesel, M. Kim, C. Lämmerzahl, A. Lambrecht, M. Mazilu, G. J. Milburn, H. Müller, L. Novotny, M. Paternostro, A. Peters, I. Pikovski, A. Pilan Zanoni, E. M. Rasel, S. Reynaud, C. J. Riedel, M. Rodrigues, L. Rondin, A. Roura, W. P. Schleich, J. Schmiedmayer, T. Schuldt, K. C. Schwab, M. Tajmar, G. M. Tino, H. Ulbricht, R. Ursin, and V. Vedral, EPJ Quantum Technol. **3**, 5 (2016).

Figures

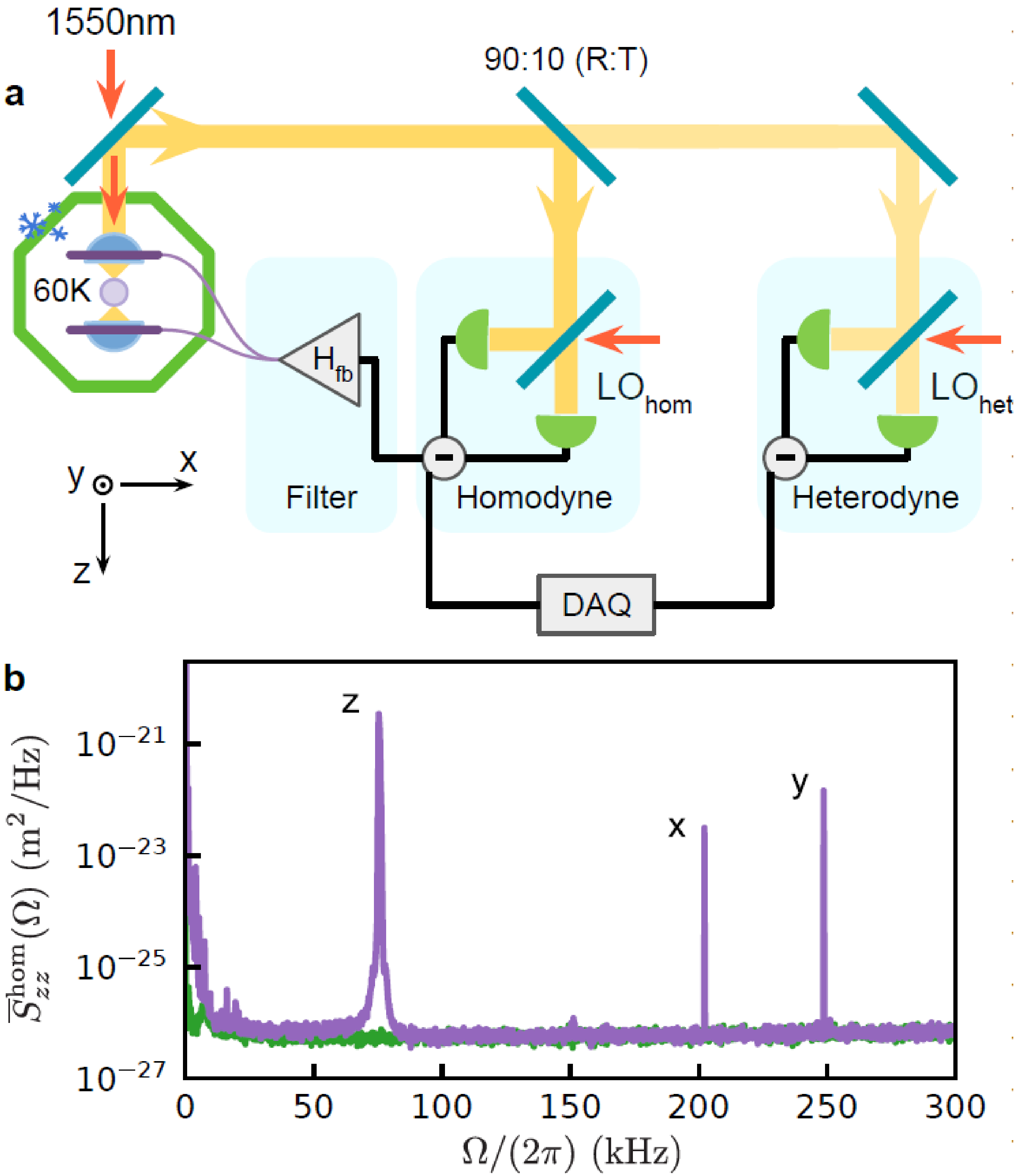

Figure 1

Experimental setup. (a) An electrically charged silica nanoparticle is optically levitated in a cryogenic environment. The light scattered back by the particle is split between the heterodyne and the homodyne receivers. The homodyne signal is filtered, and fed back as an electric force to the particle to cool its center-ofmass motion along the optical axis. (b) Power spectral density of the parametrically pre-cooled center-of-mass oscillation modes (purple) along the z, x, and y axis (at 77 kHz, 202 kHz, and 249 kHz, respectively). In green we plot the LO noise floor.

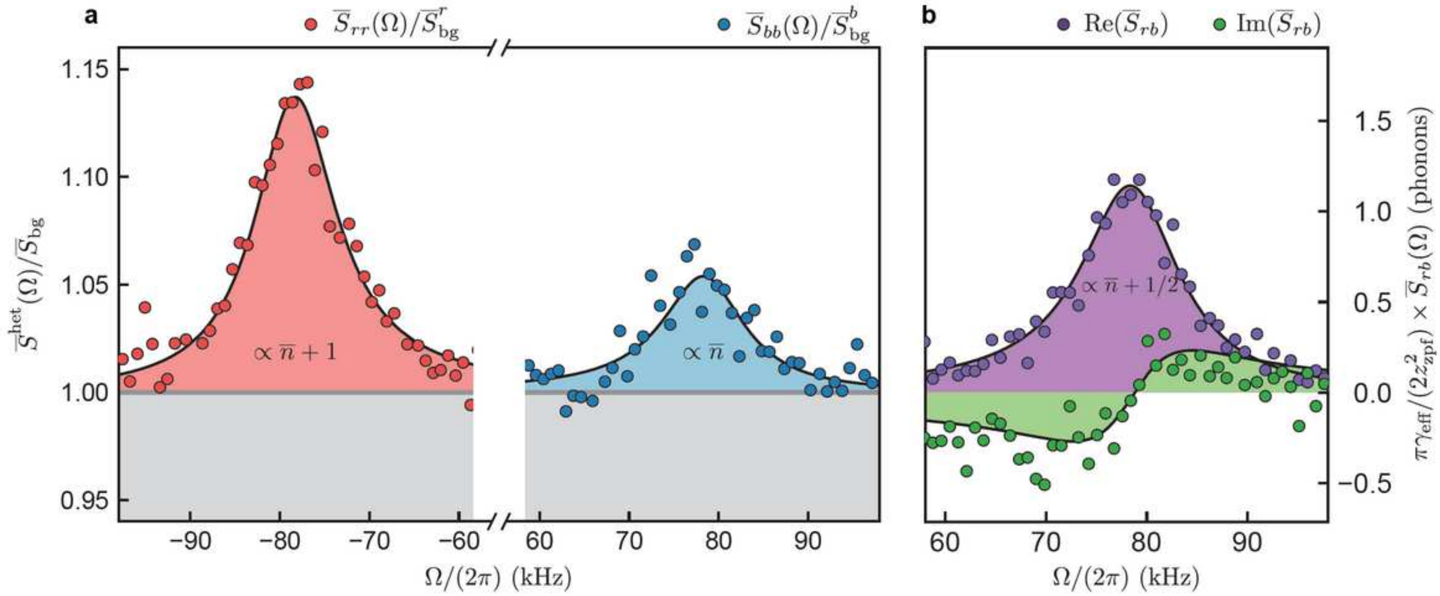

Figure 2

Quantum ground state verification via out-of-loop measurements. (a) Stokes (red circles) and anti-Stokes (blue circles) sidebands measured by the out-of-loop heterodyne detector, at the largest electronic feedback gain. The black lines are fits to Eqs. (1), from which we extract the sideband powers. From their ratio, we extract a final occupation of n¯ = 0.66 ± 0.08. (b) Real (purple circles) and imaginary (green circles) parts of the cross-power spectral density between the Stokes and anti-Stokes sideband, together with theoretical fits (black lines). We calibrate the vertical axis using the imaginary part, and we extract a final occupation of n¯ = 0.64 ± 0.09 from the real part.

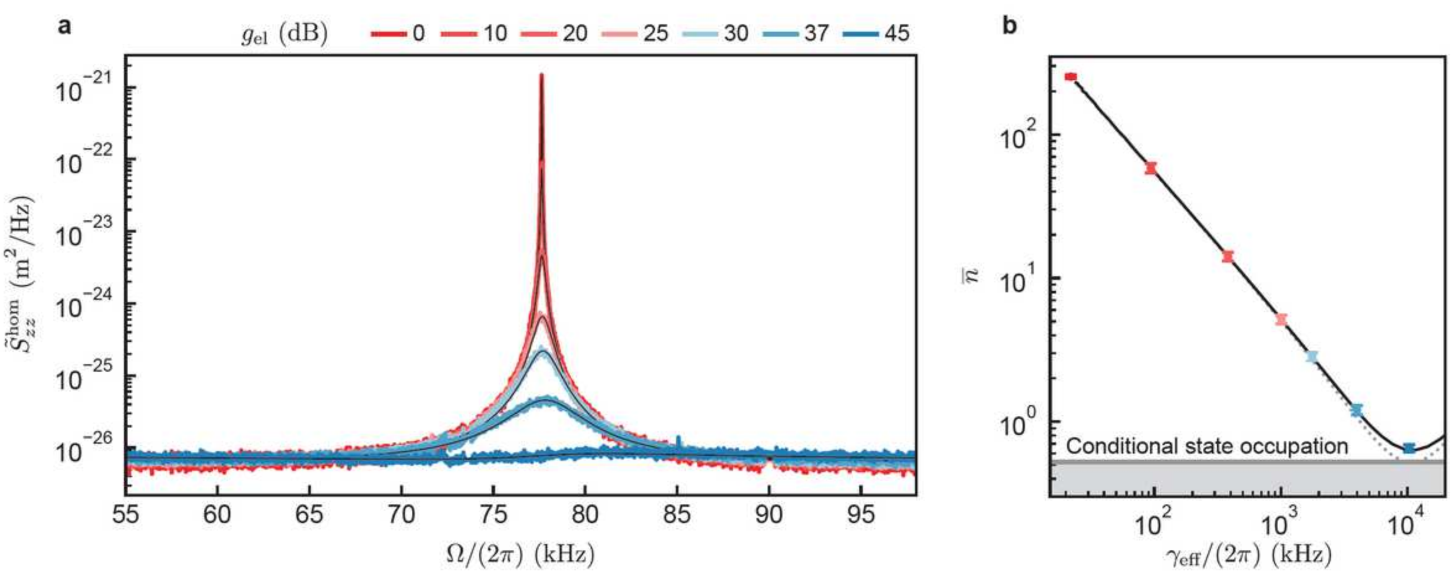

Figure 3

In-loop analysis of the feedback system. (a) Single-sided displacement spectra measured by the in-loop homodyne detector, at different electronic gains gel. We exclude three narrow spectral features from the analysis (see Supplementary). The black lines are fits to a theoretical model (see Supplementary). (b) Mechanical occupations extracted from integrating the computed position and momentum spectra, which are based on parameters estimated from the in-loop spectra. The solid black (dotted grey) line is a theoretical model assuming an ideal delay filter (cold damping). The horizontal grey line corresponds to the occupation of the conditional state, stemming from the performed measurements. The error bars reflect the standard deviation (s.d.) in the fitted parameters, as well as the statistical error on the calibration method.

Supplementary Files

This is a list of supplementary files associated with this preprint. Click to download.

- supplement.pdf